# 1 H magic-angle spinning NMR evolves as a powerful new tool for membrane proteins

Tobias Schubeis, Tanguy Le Marchand, Loren B Andreas, Guido Pintacuda

# $^{1}$H Magic-angle Spinning NMR evolves as a powerful new tool for membrane proteins

Tobias Schubeis,[a] Tanguy Le Marchand,[a] Loren B. Andreas[b] and Guido Pintacuda[a,*]

[a] Centre de RMN à Très Hauts Champs, Institut des Sciences Analytiques (UMR 5280 – CNRS, ENS Lyon, UCB Lyon 1), Université de Lyon, 5 rue de la Doua, 69100 Villeurbanne (France)

[b] Max Planck Institute for Biophysical Chemistry, Am Fassberg 11, D-37077 Göttingen, Germany

* Corresponding author: guido.pintacuda@ens-lyon.fr (Guido Pintacuda)

## Abstract

Building on a decade of continuous advances of the community, the recent development of very fast (60 kHz and above) magic-angle spinning (MAS) probes has revolutionised the field of solid-state NMR. This new spinning regime reduces the $^{1}$H-$^{1}$H dipolar couplings, so that direct detection of the larger magnetic moment available from $^{1}$H is now possible at high resolution, not only in deuterated molecules but also in fully-protonated substrates. Such capabilities allow rapid "fingerprinting" of samples with a ten-fold reduction of the required sample amounts with respect to conventional approaches, and permit extensive, robust and expeditious assignment of small-to-medium sized proteins (up to ca. 300 residues), and the determination of inter-nuclear proximities, relative orientations of secondary structural elements, protein-cofactor interactions, local and global dynamics.

Fast MAS and $^{1}$H detection techniques have nowadays been shown to be applicable to membrane-bound systems. This paper reviews the strategies underlying this recent leap forward in sensitivity and resolution, describing its potential for the detailed characterization of membrane proteins.

## Graphical TOC

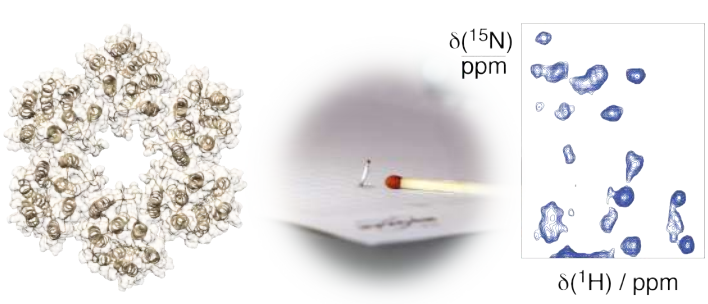

## 1. Introduction

Membrane proteins are an important class of biomacromolecules, comprising roughly 30% of the proteome. They are responsible for many critical cellular processes, including signaling across cell membranes and both passive and active ion and small molecule transportation. It is no surprise that so many drugs and drug candidates target membrane proteins.

Unfortunately, membrane proteins pose a particular challenge in structural biology. They are often difficult to express, and even when they can be produced in large amounts, they are often refractory to standard techniques. Obtaining high quality crystals in detergent or lipid cubic phases for X-ray diffraction studies remains a difficult undertaking, and solution NMR investigations are easily jeopardized by the slowly tumbling rates of the micellar preparations. Recently, developments in cryo-electron microscopy have led to an explosion in structures for larger proteins, above about 100 kDa in size, however this technique has difficulties below about 50-100 kDa.

In the last two decades, Magic Angle Spinning (MAS) NMR has developed as a generally applicable structural biology technique, capable of complementing liquid-state NMR, X-ray crystallography and electron microscopy. Following seminal work on microcrystalline proteins [1], a growing number of studies demonstrates the utility of MAS to calculate three-dimensional structures and to determine dynamics of complex assemblies such as amyloid fibrils [2-5] bacterial virulence factors [6] and intact viral capsids[7, 8]. In this context, a variety of reports have been published for membrane channels [9-16] and membrane-bound drug targets [17, 18] at an atomic level in reconstituted lipid bilayers or even directly in native cell membranes [19-21]. However, while targeted protocols have been designed for sample preparation, sequence-specific resonance assignment, and collection of conformational restraints, these procedures are still far from routine [22], and for example only for very few transmembrane proteins a complete structure determination by MAS NMR has been reported in lipid bilayers [18, 23-27].

Although the topic of this review concerns MAS, it is also important to remember that static NMR using carefully oriented sample was developed even earlier, and successfully applied to determine small alpha helical structures [28, 29]. Such studies were the first of any kind to accurately determine helical tilt angles in fluid bilayers, and also could detect the influence of protein dynamics. Nevertheless, it is our perspective that the relative ease of sample preparation and resonance assignment for MAS conditions will propel the technique to widespread use, despite missing the benefit of long-range correlation possible with oriented samples.

We have divided our discussion into the following 9 sections (2-10). In section 2 we discuss physical considerations having to do with the MAS rate, and deuteration strategies that work synergistically to narrow proton resonances. In Section 3, we discuss the problem of proton exchange in deuterated proteins, and how this can be overcome with the latest technology and labelling strategies. In section

4, we review the various methods to obtain information from protein side-chains. In section 5, we discuss the resolution and sensitivity of membrane samples in relation to current and future instrumentation. Section 6 details the workflow for sample preparation, and the advantages of sample optimization using fast MAS conditions. Section 7 and 8 review resonance assignment and structure determination, respectively. Finally, section 9 concerns measurement of dynamic processes that can be efficiently measured using 1H detection, even for bilayer embedded membrane proteins, as highlighted by several recent reports.

## 2. Proton detection, deuteration, faster MAS

Most of the biomolecular studies by MAS-NMR performed so far are primarily based on double and triple resonance spectra, making use of $^{13}$C-detected correlations between $^{13}$C and $^{15}$N signals under relatively slow MAS [30, 31]. Most transporters and membrane-bound enzymes are predicted to contain more than 6 transmembrane α-helices or 8 β-strands (>20 kDa). The resonance assignment of a protein in this size range requires the acquisition of a large set of multidimensional spectra. The long acquisition times required for $^{13}$C-detected strategies are thus a severe obstacle to the study of such proteins by MAS NMR. This is mainly due to the fact that $^{13}$C-detected experiments are relatively insensitive, in contrast to the standard solution NMR acquisition and analysis protocols, where $^{1}$H-detected triple-resonance pulse schemes provide rapid sequential assignment and structural determination [32, 33].

To extend the applicability of MAS-NMR to the detailed characterization of membrane proteins requires a leap forward in sensitivity and resolution, and many strategies have been employed over the last two decades to achieve this.

The direct detection of proton coherences, exploiting the high gyromagnetic ratio and abundance of proton nuclei, is the most natural way to enhance the spectral sensitivity [34, 35]. The very same high gyromagnetic ratio and abundance, coupled to the small spectral dispersion of $^{1}$H resonances, however generates a network of strong dipolar couplings which results in severe line-broadening at moderate (10-20 kHz) MAS rates, preventing the straightforward application of $^{1}$H detection to proteins in the solid state.

Figure 1 provides an overview of the efforts of numerous groups to overcome these challenges. Despite encouraging proof-of-principles on fully-protonated model systems [36], the most commonly used strategy to retrieve resolution has been proton dilution [37, 38].This is typically achieved by perdeuteration and back-protonation at the exchangeable sites in a suitable $H_2O/D_2O$ mixture, so that the network of strong $^{1}$H-$^{1}$H dipolar couplings that broaden the NMR signals is broken [39, 40]. Following up on pioneering studies on microcrystalline proteins, Linser *et al.* presented the first high-resolution $^{1}$H-$^{15}$N correlation spectra of two membrane proteins in lipid bilayers, the outer membrane

protein G (OmpG) and bacteriorhodopsin (bR) [41]. For these systems, the highest resolution was obtained combining 10-20 kHz MAS with extreme dilution of the proton content in the sample by chemical exchange in 10-40% $H_2O/D_2O$. With such an approach, however, the optimal deuteration level is a trade-off between high resolution and detection sensitivity, as increased dilution results in a loss of signal of the observed nuclei, in particular for $^1H$-$^1H$ correlations [42].

Figure 1 here

In parallel, the first encouraging studies on the effects of rapid sample rotation on $^1H$ resonances have driven the development of probes capable of faster MAS, which have been increasingly more effective in averaging $^1H$ dipolar interactions [34, 35]. At faster MAS rates and high magnetic fields, the proton dilution requirements become less stringent, and $^1H$ detection techniques were shown to be applicable to a seven-helical integral membrane proton pump, proteorhodopsin (PR) [43], and the four-helical transmembrane domain DsbB [44], with high reprotonation levels (70-100%) in the 30-40 kHz MAS range.

At 60 kHz MAS, sensitive cross-polarization (CP) HSQC spectra with $^1H^N$ linewidths of about 100 Hz were obtained for uniformly [$^2H$,$^{13}C$,$^{15}N$]-labeled microcrystalline protein samples fully back-exchanged at amide sites [45, 46]. Despite substantial reduction of the sample amount (to 2-3 mg for a 1.3 mm rotor), this enables the acquisition of $^1H$ resonances with extremely high spectral resolution and high signal sensitivity, as reviewed recently [47].

An increase in the spinning rate requires reduced sample dimensions, which in principle entails a major loss in sensitivity. Interestingly, the loss in sample volume is partially offset by the increased detection sensitivity associated to improved inductive coupling of smaller coils, and most importantly is compensated by the significantly longer coherence lifetimes which can be obtained with fast spinning. Longer coherence lifetimes translate into narrower proton lines and improved coherence transfer efficiencies, with improved sensitivity and resolution in multidimensional correlation experiments [48], in particular those involving many coherence transfer steps (see section 7).

Such capabilities not only allow rapid “fingerprinting” of samples but also permit extensive, robust and expeditious assignment [49], and the determination of structurally important parameters such as inter-nuclear proximities and local dynamics [50]. Notably, this approach was shown to be applicable to small-to-medium sized transmembrane systems, and for example highly resolved spectra from the influenza A M2 channel in reconstituted lipid bilayers were obtained with complete backbone assignments determined from a single sample of 1.5 mg and only two weeks of experimental time [49]. These developments speed up by almost two orders of magnitude the analysis of membrane proteins in lipid bilayers, and more complex targets of higher molecular weight, such as OmpG [49,

51], the β-barrel Outer Membrane Protein from *Klebsiella pneumoniae* (KpOmpA)[52] or the human voltage dependent anion channel (VDAC) [53], have already been reported.

The advent of even faster MAS rates in smaller rotors has reduced further the amount of sample required, and larger sensitivity gains per sample volume have been reported (0.5 mg or less is required for 0.8 mm and 0.7 mm rotors) [54-59].

## 3. Solvent accessibility and H/D exchange issues

Combined with MAS, deuteration is still the most effective way to improve resolution [60] without compromising the sensitivity of the remaining protons. Protein deuteration requires expression in $D_2O$, which reduces the protein yield in bacteria and is incompatible with certain expression systems, *e.g.* insect or mammalian cells. If feasible, NMR spectra of folded proteins might still suffer from incomplete re-protonation at the exchangeable sites during purification. This problem is particularly relevant for membrane proteins, which often lack refolding protocols, so that the reintroduction of protons is limited to exchangeable and solvent accessible sites, with a drastic loss of information for the extensive hydrophobic transmembrane regions shielded by the lipids or detergents.

This effect may be used in a constructive way. For example, Ladizhansky and coworkers have exploited this phenomenon to study the solvent-exposed regions of Proteorhodopsin (PR) [43]. PR samples were prepared by growing the apoprotein in a fully deuterated medium and reintroducing $^1H$ species to solvent-accessible sites through exchange with a 40% $H_2O/D_2O$ mixture. Only the residues susceptible to H/D exchange were observed by $^1H$-detected spectroscopy. Beside those located at the membrane interface, most of the observed resonances clustered within a particular transmembrane helix. This result was used to prove transient exposition of a hydrophilic cavity in the extracellular half of the protein, an aspect related to proton conduction.

In another recent example, incomplete H/D exchange in the transmembrane region was used as a tool for improved $^1H$ resolution of water-inaccessible protein regions [61]. Incubation in $D_2O$ of an inverse fractional deuterated sample (approximately 30% overall deuteration, see below) of the $K^+$-channel KcsA, produced the complete disappearance of the water-exposed residues, with a substantial enhancement in spectral quality at 60 kHz MAS. Additionally, the $D_2O$ wash removed any residual dipolar couplings to water protons from large internal water-filled cavities and buried waters, further narrowing the $^1H$ linewidths (Figure 2).

Figure 2 here

A more general solution to avoid incomplete back-exchange of amide $^1Hs$ is application of >100 kHz MAS, which releases the need for proton dilution and enables the acquisition of resolved $^1H$,$^{15}N$ fingerprints from fully-protonated samples [58]. In the case of PR, the resolution of a $^1H$-$^{15}N$

correlation acquired on a fully-protonated sample at 100 kHz was virtually identical to that of a perdeuterated and 100% amide-reprotonated sample at 60 kHz (Figure 3) [62]. As observed earlier by Ladizhansky and coworkers [43], several amide groups engaged in hydrogen bonds in hydrophobic transmembrane regions are not detected in the deuterated sample, as they are inaccessible to proton exchange. In contrast, the ubiquity of $^{1}$H species in fully protonated PR allows the entire molecule to be probed, in particular moieties from the most structured regions of the protein. With the study of samples directly expressed in 100% $H_2O$, $^{1}$H-detected structural determination are thus extended to exchange-protected transmembrane regions.

Figure 3 here

## 4. Side chains protons and tailored labeling schemes

The perdeuteration and exchange approach severely limits observation of side-chain signals, which are essential reporters of structure, dynamics and interactions in a protein. In contrast to amide sites, introduction of protons or deuterons in side-chains can only take place during protein expression (Asn, Gln, Ser, Thr, Trp, His –OH, -NH and $–NH_2$ side chain protons are exceptions, but often suffer from exchange broadening). The simplest route to diluting side-chain protons is therefore to perform protein expression using $^{2}$H,$^{13}$C-glucose and controlled low concentration (5-15%) of $H_2O$ in a $D_2O$ buffer, an approach termed Reduced Adjoining Protonation (RAP) [63], or using $^{1}$H,$^{13}$C-glucose in $D_2O$ media, in the so-called Fractional Deuteration (FD) [64]. This latter strategy was applied to the ion channel KcsA [65] and to the outer-membrane protein Ail [66], and resulted in the random incorporation of protons at a level of 10-40% into deuterated protein matrices. Combined with fast (55 kHz) spinning, this yielded aliphatic $^{1}$H linewidths between 25 and 60 Hz, a resolution compatible with their site-specific assignment and their constructive use for structural studies.

In this approach, however, resolution relies on a low site occupancy of aliphatic protons, which impacts sensitivity and offsets the advantages of $^{1}$H-detection [67]. An alternative concept, developed originally for liquid-state NMR, consists in supplementing a deuterated expression medium with suitably labelled metabolic precursors for I, L, V residues, providing stereospecific $^{13}C^{1}HD_2$-labelling with 100% occupancy for these three residue types [68]. At 60 kHz MAS, this yielded an extremely well resolved $^{1}$H,$^{13}$C methyl fingerprint for the conductance domain of M2 from influenza A, which was the basis for the extraction of inter-helix $^{1}$H,$^{1}$H contacts in the four-helix bundle (Figure 4a) [27]. A similar approach, referred to as proton-cloud labeling, consists in the incorporation of specific fully-protonated amino acid into an otherwise deuterated matrix [69]. The method is amenable to almost all amino acids outside of the citric acid (TCA) cycle. Simultaneous reduction of proton line-

widths and spectral crowding were reported for a V,L,K $^{1}$H-cloud labelled sample of membrane-embedded BamA, a component of the β-barrel assembly machinery (Figure 4b).

Figure 4 here

All the methods mentioned above, however, share the common need of expression in highly concentrated $D_2O$, a procedure that as discussed earlier slows down bacterial growth, lowers the expression levels, and is incompatible with some expression systems. A first solution to this issue, proposed by Medeiros-Silva and coworkers, consists in a minimal expression medium composed by $^{2}$H-glucose in $H_2O$ (inverse Fractional Deuteration, iFD) [61]. The resulting samples feature low (10-40%) deuterium levels, but remarkable resolution enhancements with respect to fully-protonated samples at 60 kHz MAS. In the case of the ion channel KcsA, iFD notably provided access to backbone and side-chain resonances in transmembrane regions (Figure 4c). In this scheme, however, the improved $^{1}$H resolution is offset by an increased broadening of the $^{13}$C resonances (the isotope shift is about 0.25 - 0.3 ppm per attached $^{2}$H) due to the $^{1}$H/$^{2}$H isotopomeric distributions from side-chain moieties [60].

This drawback is overcome if resolved side-chain proton resonances are available from a fully protonated sample, which is by far the easiest and least expensive to obtain. While 30-60 kHz MAS provided only limited resolution in $^{1}$H side-chains in conjunction with full protonation [36, 70-72], the recent development of MAS at above 100 kHz has produced a dramatic reduction in homogenous line broadening to improve the resolution of $^{1}$H resonances, enabling the detection of alpha and side-chain protons at a resolution comparable with those of the amide groups in deuterated samples at slower MAS [58, 73]. Resolved two dimensional $^{1}$H,$^{13}$C fingerprints have been demonstrated both on α-helical [62] and β-barrel type proteins in lipid bilayers (Figure 4d and e), opening unprecedented opportunities for structural investigations of membrane proteins by using sensitive $^{1}$H-detected methods.

## 5. Resolution and sensitivity

Membrane-embedded proteins are a challenging class of samples due to an inherent dilution of protein in lipids, and the potential for intrinsic static and dynamic disorder, as compared with microcrystals. It is therefore important to carefully consider the magnetic field and the spinning frequency that will optimize effective data acquisition due to their impact on linewidth and sensitivity. The linewidth is a convolution of inhomogeneous and homogeneous contributions. The inhomogeneous component is the result of both imperfect magnetic field homogeneity, as well as static disorder in the sample. The homogeneous contribution to the line, on the other hand, arises from imperfect decoupling of dipolar interactions by MAS as well as dynamic processes. Only the

homogeneous component can be decreased by faster MAS and higher fields. While microcrystalline proteins usually exhibit a small inhomogeneous contribution, for membrane proteins, even in carefully optimized 2D-crystals, it is usually substantial (0.1-0.2 ppm). For example, for PR at 100 kHz MAS and using a 1 GHz spectrometer, there are approximately equal contributions from homogeneous and inhomogeneous sources with each contributing about 140 Hz [62]. Even if this limits the possible gains in resolution attainable for this kind of samples, significant line narrowing is still expected from reduction of the homogeneous contribution.

The sensitivity loss due to the decrease of the sample amount accommodated in a smaller rotor is partially compensated by the reduction of the detection coil diameter and the linewidth of detected $^{1}$H nuclei [34]. For multidimensional spectra, the sensitivity benefits from longer coherence lifetimes at fast MAS, due to the reduction of the irreversible signal decay during magnetization transfer. It is therefore observed that a decrease in the rotor size can result in decreased sensitivity in simple 1D spectra, but improved sensitivity in more complex multidimensional [48].

Although the most obvious effect of magnetic field is that the sensitivity scales up with the field ($B_0$), as $B_0^{3/2}$, it also affects both the homogeneous and inhomogeneous linewidths (in Hz). High magnetic fields help to separate heavily overlapped proton resonances of dipolar coupled protons, thus reducing $^{1}$H relaxation driven by spin flip-flops [67]. We therefore expect that further increases in the magnetic field, which will narrow the homogeneous linewidth and at the same time improve sensitivity, will be particularly important in the future. We anticipate that a further step forward in increasing $B_0$, and thereby sensitivity, will work synergistically in order to fully benefit from the future resolution gains expected from faster MAS probes.

## 6. Membrane protein preparation and sample screening

Using solid-state NMR, membrane proteins can be analyzed in native or native-like lipid bilayer environments. Considering the complexity of structural and dynamical investigations, starting with an optimal sample is absolutely crucial.

The main steps of sample optimization involve the establishment of a robust expression system, the development of protocols for the purification in detergent, and the setup of suitable activity assays. These phases are common to the structural characterization of membrane proteins by any biophysical technique. For solid-state NMR studies, they are followed by the reconstitution of a monodisperse and active membrane protein sample from detergent micelles into lipids, which requires several additional screening steps [74]. The basic concept is to mix lipids with a detergent solubilized membrane protein and remove the detergent to achieve incorporation of proteins into the lipid bilayers. The method of choice for detergent removal depends largely on the detergent. Detergents with a small micelle size or high critical micelle concentration (CMC), such as octyl glucoside (OG),

can easily be removed by dialysis. For other detergents with a very low CMC, such as β-dodecyl-deoxymaltoside (DDM), hydrophobic beads or detergent-entrapping molecules, such as cyclodextrin, are generally employed. Commonly used lipids have a fatty-acid chain length ranging from 14 to 18 carbon atoms, and a polar head group consisting of phosphatidyl-choline, -ethanolamine or -serine. Many phospholipids are also available with high degrees of deuteration which removes background proton signals and may facilitate for example the assignment of protein side chain resonances.

Finally, once membrane proteins are incorporated into lipid bilayers, the preparation forms a turbid film that can be sedimented by ultracentrifugation. The development of specialized ultracentrifuge tools (*e.g.* spiNpack by Giottobiotech) allows the sedimentation step to be performed while directly filling the MAS NMR rotors [75, 76]. Proteins that are highly sensitive to their environment might require a deeper analysis for its lipid composition and detergent removal e.g. by evaporative light scattering [77].

While this reconstitution procedure is nowadays well-established, and detailed instructions can be found in the literature, the quality of the NMR spectra depends on several factors that need to be optimized, namely the type(s) of lipid, the lipid-to-protein ratio and the temperature during both reconstitution and the NMR measurements. The lipid composition of many viral, bacterial as well as eukaryotic cell membranes have been thoroughly studied and membrane protein samples for solid state NMR should optimally closely reproduce the native environment. At the same time, some compromise must be made, since nearly all proteins cannot be detected my NMR at native concentrations. Some researchers favor native lipids, while others turn to Liposome based activity assays to establish suitable *in vitro* conditions, since the average lipid composition may not reproduce the environment *in vivo*. Samples optimized to match *in vivo* and functional conditions may or may not lead to sharp resonances in NMR, depending on the structural ensemble present in near-native states. Samples can also be optimized iteratively using NMR, and even though the best NMR sample does not always represent the most native state, such bilayer preparations will likely represent a state that is a valuable starting point for further study.

With traditional heteronuclear-detected methods, sample screening represents a very time and resources consuming task. Each tested condition requires ~10 mg of sample, and its quality is established by either one dimensional $^{15}$N spectra, which are extremely insensitive, or by two dimensional $^{13}$C-$^{13}$C or $^{13}$C-$^{15}$N correlations, which facilitate the analysis but make the screening very costly if the expression yields are not far above average.

The use of smaller 1.3 mm rotors at 60 kHz MAS provides a substantial step forward in this procedure, as it permits screening of sample conditions by 2D $^{1}$H-$^{15}$N correlation spectra using only 1-2 mg of $^{15}$N labeled protein. Information-rich fingerprint spectra can be recorded in a matter of hours, thus increasing the sample throughput significantly.

Figure 5 here

An example of NMR-based sample optimization is illustrated in Figure 5 for the case of the outer membrane protein AlkL [78]. It starts with testing different lipids or lipid mixtures at a lipid-to-protein ratio of 1:1 (w/w), and comparing 2D spectra recorded at different temperatures in the 5-35°C range. Poor preparations feature either only few resonances (Figure 5a), indicating that most signals are broadened beyond detection, or a single unresolved intensity, associated with the presence of multiple static conformational states. The first striking indication of conditions suitable for NMR is the appearance of isolated signals with homogeneous intensities and linewidths at the edge of the spectrum, for example in chemical shift regions corresponding to specific aminoacids, such as *e.g.* Glycine or Tryptophan side chains as shown in Figure 5 b. Once a suitable lipid or lipid mixture has been identified, the lipid-to-protein ratio is reduced stepwise in order to increase the sensitivity of the NMR experiments, and 2D spectra are used to determine the lowest lipid-to-protein ratio compatible with high resolution. In this phase, not only the lineshapes, but also amide proton and nitrogen coherence lifetimes ($T_2$') can be measured, and used as criteria to assess the sample quality. This optimal lipid-to-protein ratio allows the acquisition of high quality NMR spectra in the shortest time, as shown in Figure 5c, which is especially important for a subsequent full NMR characterization requiring the acquisition of 3D correlations. Finally, optimized preparations are packed into 0.7 mm rotors (1.3 mm rotors when/if partial deuteration is possible) to perform experiments with today's highest possible resolution at the highest magnetic field (Figure 5d).

## 7. Backbone and side-chain resonance assignments

Resonance assignment represents the basis for any site-specific protein NMR investigation of biophysical properties, such as structure, dynamics, interactions, and solvent exposure. The availability of fast MAS probes has revolutionized this procedure, allowing the establishment of a comprehensive and robust methodology for achieving rapid resonance assignments that takes into account all backbone chemical shift sources in $^{1}$H-detected magic-angle spinning NMR spectra [49, 79].

Once suitable measurements conditions have been established, $^{1}$H-detected sequential resonance assignment can be tackled with the use of higher-dimensional spectra, where the $^{1}$H-$^{15}$N correlation module is complemented with heteronuclear H/C and N/C CP steps, to allow recording an extra $^{13}$C dimension. The simplest 3D spectra, (H)CONH and (H)CANH, correlate the $^{1}$H and $^{15}$N shifts with those of the neighboring $^{13}$C' and $^{13}$CA spins, respectively, and typically provide nearly full site-specific resolution in only a few hours for proteins in a range up to nearly 300 residues [80]. Site-specific resonance assignment is based on the acquisition of pairs of spectra linking the $^{1}$H/$^{15}$N shifts of adjacent residues over the CO, CA or CB resonances. Overall, a set of six 3D correlations has been

proposed[49], where the basic (H)CONH and (H)CANH experiments are supplemented with additional experiments which include C-C coherence transfers along the protein backbone [46]. Homonuclear carbon-carbon transfers are best performed through dipolar couplings in the 30-40 kHz MAS regime [44], while scalar-based transfers become competitive at 60 kHz MAS and above [81]. One, two, three transfers result in the (H)CO(CA)NH [46], (H)(CO)CA(CO)NH and (H)(CA)CB(CA)NH [82], and (H)(CA)CB(CACO)NH [49] experiments, respectively. The $^{13}$CA and $^{13}$CB shifts allow identification of the residue types, and joint analysis of the set of six spectra yields backbone resonance assignment by simultaneous matching of the three independent $^{13}$C (CO, CA and CB) chemical shifts. This accelerates and strengthens the reliability of backbone sequential assignment, enabling at the same time the use of unsupervised state-of-the-art computational data analysis protocols originally developed for solution NMR [83, 84]}. In addition to this set, amide linking in (H)N(CACO)NH and (H)N(COCA)NH spectra can provide additional redundant linking to resolve ambiguities of heavily overlapping regions, due to the low correlation among sequential amide shifts [56, 85].

In comparison to $^{13}$C-based methods, this approach reduces by one order of magnitude the experimental acquisition times and the sample amounts necessary, and as such represents a quantum leap forward for biological solid-state NMR structure determination of proteins in the solid state.

Although this assignment strategy was initially optimized for deuterated and 100% amide-reprotonated samples in microcrystalline form at 60 kHz MAS, the approach remains successful for the assignment of a number of non-crystalline small-to-medium sized systems. Notably, backbone assignments were readily established for M2 (2x43 residues) [27, 49]and for considerable portions of OmpG (280 residues) [49] and kpOmpA (210 residues), [52] after acquisition of each set of six spectra in 2 weeks on the 1 GHz spectrometer, on samples containing about 1 mg of protein.

As discussed above, using $\geqq$100 kHz MAS, these same correlation experiments are equally efficient for sequential resonance assignment of fully-protonated samples [58]. In this spinning regime, the α-proton resonances also feature high spectral resolution, comparable to amide protons, but less affected by sample inhomogeneity. We therefore designed a suite of four 3D experiments that employ a $^{13}$Cα-$^{1}$Hα correlation as the detection scheme [73]. The first pair, (H)N(CO)CAH and (H)NCAH, records inter- and intra-residue correlations, respectively. These allow to sequentially link Cα-Hα resonance pairs by matching a common $^{15}$N chemical shift. The second pair, (H)CO(N)CAH and (H)COCAH, links sequential Cα-Hα groups based on correlations to a common $^{13}$C′ chemical shift. Simultaneous matching of $^{15}$N and $^{13}$C′ chemical shifts resolves ambiguities and ensures high reliability of the sequential assignment.

For fully-protonated proteins, these Hα-detected experiments can be used in addition to the $H^N$-detected sequences, making up a larger palette of datasets that increases the level of redundancy necessary for residue linking and shifts its applicability to larger proteins.

Alternatively, a subset of the most sensitive (and therefore most complete) experiments could be sufficient for a complete assignment of a medium-size target, with a judicious selection to be performed on a case-by-case basis. As reported recently in the case of PR, for example, short coherence lifetimes where observed for $^{13}$Cα spins, while those of $^{13}$C' spins were significantly longer, so the pair of $H^N$-detected sequences for $^{13}$Cα matching and the pair of Hα-detected sequences for $^{15}$N-matching were the preferred choice, as they had higher transfer efficiencies and significantly shorter acquisition times (Figure 6)[62].

Figure 6 here

Finally, resolved signals for the Hα and Cα resonances are used as anchors to propagate resonance assignment from backbone to side-chains. This can be performed by inserting in the $^{1}$Hα-$^{13}$Cα correlation module a $^{1}J_{CC}$-mediated $^{13}$C-$^{13}$C isotropic mixing (e.g. WALTZ-16), which ensures exchange of magnetization between side-chain $^{13}$C nuclei [58, 73]. The resulting datasets correlate aliphatic side-chain $^{1}$H or $^{13}$C resonances of a given residue to each directly bonded spin pair (such as Hα-Cα, Hβ-Cβ,…), confirming the identification of the amino acid types and at the same time yielding the assignment of the $^{1}$H and $^{13}$C side-chain resonances.

## 8. Structure investigation

Effective structure determination by NMR demands high sensitivity and resolution, and it is no surprise that much of the work over the last decade has been dedicated to optimization of data acquisition to improve both. This work is ongoing, but has been successful enough for application to several membrane protein systems, both for complete or partial structure determination.

The most established approach relies on $^{13}$C detection, using 3.2 mm rotors, often with RF circuit designs that reduce the electric field in the sample area for the proton frequency [86]. This is important, particularly at high magnetic field, to limit sample heating due to RF pulses.

Following the progress described in the previous sections, rotors with a diameter of 0.6 to 1.3 mm are slowly becoming the 'go-to' choices for structural measurements in biological systems, as it enables resolved proton spectra, and reduced sample amounts. At the current time, both strategies are in use, and sometimes applied together for structure determination.

Here we focus on the contribution of proton detected spectra for structure determination. Structural data for relatively few membrane proteins have been reported thus far, although high quality proton

spectra have been reported for additional examples. Currently there is substantial structural data (contacts between residues separated by more than 4 in the sequence) for M2 (5 kD)[27], OmpG (30 kD) [51]PR (30 kD) [62] and AlkL (22 kD) [87]. Spectra of other membrane proteins are of similar quality, such as VDAC [53] or KcsA [65], for which through space transfer between sequential residues was observed.

The M2 protein from influenza A is 97 residues, and a key function of the protein is to conduct protons at low pH, which triggers membrane fusion in late endosomes and release of viral RNA. The protein has a single pass alpha helix that assembles as tetramers in membranes, as well as a short amphipathic helix on the C-terminal side. The protein has received considerable interest since it was discovered as the target of aminoadamantyl inhibitors amantadine and rimantadine, which were once effective therapeutic agents, but which have been rendered ineffective due to widespread resistance mutations. Many structures have been deposited in the pdb by a variety of methods, including oriented sample NMR [88], X-ray diffraction [89] and solution NMR [90], yet a consensus in the detailed structural features is not evident, pointing to a sensitivity of the structure towards the sample conditions and the choice of protein construct. A MAS structure [27] of the drug-resistant S31N M2 utilized a combined strategy, using both carbon and proton detection. While the majority of structural restraints came from $^{13}C$ detection, an overwhelming majority of data acquisition was also dedicated towards that strategy. Importantly, the proton detected data provided a more redundant and reliable backbone assignment [49]. Additionally, His and Trp residues are structured in the core of the tetrameric bundle, and are the key conserved residues that are responsible for controlled pH sensitive conduction. Detection of protons allowed the measurement of important distances among the indole and imidazole protons (Figure 7a-b).

Figure 7 here

PR is an alpha helical membrane protein of 7 transmembrane (TM) helices, and a chromophore is the heart of this light-driven ion pump. The protein shares its topology with other 7 TM g-protein coupled receptors (GPCRs), an important class of proteins that are the target of many drugs and drug candidates. The Ladizhansky group showed that the protein is highly ordered when reconstituted in DMPC/DMPA membranes, as indicated by highly resolved $^{13}C$ and $^{15}N$ spectra [43]. Using $^{13}C$ detection, they were able to extensively assign the protein, and to use the assignments as a sensitive probe of structure and dynamics. We recently applied 100 kHz MAS at a proton frequency of 1 GHz in order to record and assign narrow proton resonances, both amides, as well as aliphatic protons [62]. Using $^{1}H$-$^{1}H$ Radio-Frequency Driven Recoupling (RFDR) mixing for magnetisation transfer, it was possible to observe cross-peaks from backbone to aliphatics and among aliphatics in a 3D $^{13}C$-edited spectrum, which report on crucial inter-residue proximities for defining the fold of an α-helical

bundle. Additionally, signals assigned to protein-cofactor contacts were also detected, providing important structural restraints in the heart of the ion pump at the functional retinal cofactor.

Proton detection is also an effective strategy for beta barrel membrane proteins. Using perdeuteration and back exchange, proton resonances below 0.2 ppm were recorded for VDAC, and as expected, many of the cross-peaks were identified based on the CA-N projection of a CA-N-H spectrum [53]. The protein was prepared in lipid bilayers as 2D arrays, which results in a homogeneous environment favorable for NMR [91]. VDAC is an important mediator of ATP and ADP transport across the mitochondrial membrane, and its role in many cellular processes, as well as dysfunction, continues to be actively investigated. Although no proton detected restraints from such preparations have been recorded, the spectral quality is in line with those of the best membrane protein samples reported so far by solid state NMR.

OmpG is a bacterial beta barrel that may form a non-specific channel [92]. Similar to VDAC, 2D arrays of OmpG can be prepared in lipid bilayers [93], and yield well resolved proton, carbon, and nitrogen spectra. A combined approach was used for structure determination, that made use of a large set of differently labeled samples and carbon-detected restrains, as well as proton-proton restraints using RFDR and detected on proton. In detail, a pair of 3D (H)NHH and (H)N(HH)NH spectra with $^{1}$H-$^{1}$H RFDR mixing was recorded for a perdeuterated and $H_2O$ exchanged sample. The proton restraints were used alone to define an initial structure, since these amide-amide restraints are particularly useful for the definition of beta sheets. In later refinement steps including many more $^{13}$C restraints, a high quality structural bundle was determined, which is largely in agreement with crystallographic data, but differs in the placement of a potentially important helix in an extracellular loop [51].

Well-resolved spectra were recorded for AlkL, a membrane protein of unknown structure [87]. The protein is predicted to be an 8-stranded beta barrel (Figure 8c), by homology with OmpW and OprG, and is important for import of alkanes and other hydrophobic molecules that can be metabolized by the intracellular membrane protein AlkB [78, 94]. We are currently assigning AlkL for mechanistic studies (both structure and dynamics) of the protein. In the meantime, we used AlkL as a model membrane protein to validate a new approach to determine proton-proton restraints, which makes use of frequency band selective recoupling to direct polarization only among a subset of all protons (Figure 7d-e). This strategy termed BAnd-Selective Spectral Spin Diffusion (BASS-SD) is important for fully protonated samples, where the magnetization otherwise ‘leaks’ to other nearby protons. At the same time, the mechanism of the transfer involves a third proton, which complicates the interpretation of the relationship between peak volumes and distance. Recoupling of a selected band of protons at the amide frequency (as done by default in deuterated and back-exchanged proteins [95]) results in a highly effective set of structural restraints across β-strands. In a similar fashion, we

anticipate that band selective recouping approaches such as BASS-SD will be generally effective in fully protonated samples.

## 9. Dynamics

Beyond structures, NMR remains the ideal tool for investigation of dynamics, since it is unique in its ability to distinguish static and dynamic disorder, and to characterize not only amplitudes, but also timescales of motion. Such possibility is particularly interesting for membrane proteins because their function often involves conformational plasticity, either for transport of small molecules, or for signaling across the membrane.

Protein dynamics based on $^{1}$H-detected NMR spectroscopy at fast MAS is a rapidly developing tool [50, 96-99]) that solves both major issues encountered at lower MAS rates. Firstly, $^{1}$H-detected NMR spectroscopy simultaneously provides the resolution and sensitivity required for the site-specific measurement of multiple observables, such as spin relaxation rates or dipole couplings, in larger proteins. Secondly, fast MAS rates alleviate potential interference from residual coherent contributions to the observed spin relaxation rates. This has made the measurement of effects such as $^{15}$N [100, 101], $^{13}$C [98] or even $^{1}$H [99] $R_{1\varrho}$ relaxation possible, progressively expanding the palette of NMR probes and spanning a timescale of events that is potentially broader than that probed by solution NMR.

While most of the recent progress has focused on microcrystalline samples, methods have progressively turned towards more heterogenous non-crystalline preparations [54, 102, 103].

Ladizhansky and coworkers were the first to demonstrate the advantages of fast MAS for the determination of conformational dynamics in the context of membrane proteins [97, 104]. They used 60 kHz MAS on a fully-protonated sample to measure site-specific $^{15}$N-$^{1}$H dipolar couplings, $^{15}$N $R_{1\varrho}$ and $^{15}$N $R_1$ relaxation rates in the seven transmembrane protein Anabaena Sensory Rhodopsin (ASR). These data were analyzed in terms of fast single site motion and local collective motions, and allowed the description of the different motional modes of the protein, with specific timescales of dynamics reported for both the TM regions and also the loops.

A seminal study on membrane protein dynamics combining fast MAS with proton-detection was performed by Weingarth and coworkers [61]. Highly resolved $^{1}$H-$^{15}$N spectra of the transmembrane part of KcsA were obtained with the iFD labelling scheme. The quality of the spectra of KcsA in lipid bilayers enabled site-specific measurements of $^{15}$N $R_{1\varrho}$ for the protein segment involved in the ion conduction, highlighting ns-$\mu$s timescale motion enhancements in this region. Interestingly, the sensitivity gain brought by proton detection also allowed acquisition of $^{1}$H-$^{15}$N correlations of KcsA in a bacterial membrane. Even if the sensitivity obtained for this low-concentration preparation was too low to measure spin relaxation, a comparison of relative cross-peak intensities suggests

modification of protein motions by going from a native environment to an artificial lipid bilayer.
Motions of the transmembrane part of kpOmpA have been recently reported [52]. Here $^{1}$H-detected NMR spectroscopy at 60 kHz MAS was used to record site-specific $^{15}$N $R_1$ and $R_{1\varrho}$ as well as $^{1}$H-$^{15}$N REDOR dipolar recoupling experiments (Figure 8). The results revealed that in the highly concentrated preparations optimized for MAS NMR uniaxial motions are abrogated, while the data are explained by residual small amplitude collective rocking motions of the β-barrel in the lipid phase. Additional contribution to the $^{15}$N $R_{1\varrho}$ relaxation rates at the edges of the strands were attributed to local flexibility. In particular, the analysis highlights the enhanced flexibility of an extracellular loop that may be involved in the process of cell adhesion, a hypothesis that was further supported by trypsin cleavage experiments.

Figure 8 here

An interesting study of membrane protein dynamics was performed by Schanda's group on the protein CzcD (2·34 kDa) in nanodiscs made of styrene-maleic acid polymer (SMA) [105]. By using proton-detected 3D experiments at 55kHz MAS with perdeuteration and back-exchange, resonance assignments were obtained for several signals, for which $^{15}$N $R_{1\varrho}$ as well as $^{1}$H-$^{15}$N REDOR dipolar recoupling data could be measured. The data not only support the absence of fast axial fluctuations, but additionally indicate that overall motions may be absent in such kind of preparations.
Finally, the connection between lipid bilayer fluidity and protein dynamics was further assessed by Meier's group with a study at 110 kHz [106]. There, spectral properties such as cross-polarization efficiencies, $^{1}$H and $^{15}$N $T_2$' and linewidths were investigated above and below of the lipid phase transition temperature as reporters of global motions for the membrane protein OmpX in nanodiscs, in both deuterated/back-exchanged and fully-protonated forms.
Overall, this fast movement forward glimpses the major role that $^{1}$H-detected NMR spectroscopy at fast MAS will play in the description of membrane protein dynamics in the near future.

## 10. Conclusions and perspectives

In conclusion, we have discussed the utility of proton detection in solid-state NMR for the investigation of membrane proteins. Although the number of examples is still small, we have highlighted recent reports that seek optimal strategies for measurement of structural and dynamical properties. It is particularly encouraging that the molecular complexity of successful examples continues to increase, such that many more important proteins can be studied, currently up to about 300 residues. The tools developed for solution NMR can often be adapted and extended for complex MAS spectra. In so doing the NMR-accessible sample repertoire has been enlarged. This is a

significant step towards routine structural, mechanistic, and dynamical investigations of large, poorly soluble and non-crystalline systems.

We expect that the trend toward higher magnetic fields will continue, and that $^{1}$H detection will be significantly improved with the next step change in field to 1.2 GHz. At the same time, faster MAS rates are also just around the corner and may enable new spectroscopy, just as previous ~2-fold steps in MAS have. We also expect that continued innovation in labeling strategies will expand the toolbox available, such that $^{1}$H detected MAS NMR becomes a highly effective strategy for the structural biologist.

## Acknowledgements

Financial support from the CNRS (IR-RMN FR3050) and from the European Research Council (ERC) under the European Union's Horizon 2020 research and innovation programme (ERC-2015-CoG GA n°648974) are gratefully acknowledged.

## Figure captions

Figure 1: Overview of $^{1}$H-detected MAS NMR approaches on membrane proteins. a) 2D $^{1}$H-$^{15}$N correlation spectra obtained in the recent literature (from refs [27, 41, 43, 44, 49, 52, 53, 61, 62, 66, 105-107]) are plotted according to the degree of protein protonation and the MAS rates applied in the study. 10, 40 and 100% $H^N$ stand for $^{2}$H labelling with, respectively, 10, 40 and 100% reprotonation at the amide sites, FD and iFD for Fractional Deuteration and inverse Fractional Deuteration, and 100% H for full protonation. b) Ribbon diagrams of protein structures for which $^{1}$H-detected MAS NMR spectra in lipids have been reported so far.

Figure 2: Inverse fractional deuteration (iFD) and bleaching of the exchangeable sites demonstrated on the $K^+$-channel KcsA reconstituted in *E. coli* polar lipids. a) 2D $^{1}$H,$^{15}$N of iFD KcsA at 60 kHz; b) 2D $^{1}$H,$^{15}$N of iFD KcsA after washing with $D_2O$; c) color coding of regions that feature detectable signals in each sample; d) assessment of $^{1}$H linewidths before (blue) and after (magenta) the $D_2O$ wash. Readapted with modification from ref [61].

Figure 3: a) Overlay of 2D $^{1}$H,$^{15}$N spectra of fully protonated $^{13}$C,$^{15}$N PR in DMPC:DMPA lipids at 100 kHz MAS (blue), and $^{2}$H, $^{15}$N, $^{13}$C and 100% back exchanged PR, in the same lipids at 60 kHz MAS (red); b) depiction on the PR structure of the amide protons in blue and red for the fully protonated and perdeuterated samples. Figure reproduced with modification from ref [62].

Figure 4: 2D $^{1}$H,$^{13}$C spectra of membrane-protein preparations with different isotopic labeling patterns. a) ILV-labelled M2; b) V,L,K $^{1}$H-cloud-labelled BamA (black dots indicate the predicted resonances using the homology model for BamA); c) iFD-labelled KcsA; d-e) fully-protonated PR and AlkL. Spectra a-c and e-f were acquired at MAS rates of 60 and 100 kHz, respectively. Readapted with modification from refs [27, 62, 65, 69].

Figure 5: Sample optimization of $^{15}$N-labelled AlkL in lipid bilayers of different compositions. a) DPhPC, protein-to-lipid ratio 1:1, b) DMPC, protein-to-lipid ratio 1:1, c) DMPC, protein-to-lipid ratio 2:1, recorded at 800 MHz with 60 kHz MAS. d) DMPC, protein-to-lipid ratio 2:1, recorded at 1000 MHz with 111 kHz MAS. Red circles highlight isolated peaks.

Figure 6: Sequential assignments of residues 172-179 in fully protonated PR in lipids bilayers. a) Diagrams of the spins for which the frequency of evolution is measured in $H^N$-detected (H)CANH ( green) and (H)(CO)CA(CO)NH (orange) experiments (left) and the Hα-detected (H)NCAHA (magenta) and (H)N(CO)CAHA (blue) experiments (right). b) Strip plots from the corresponding $H^N$-

detected (left) and the Hα-detected spectra (right). The four spectra were acquired at 100 kHz MAS and 23.5 T. Figure reprinted with modification from ref [62].

Figure 7: a-b) Gating and pH sensing residues in the influenza A M2 dimer of dimers. a) A short intermolecular distance of 3 to 3.5 Å is observed between H37 and W41; b) this proximity is confirmed in an N(H)H RFDR spectrum. c) Sequence homology prediction of secondary structure of AlkL from *Pseudomonas putida,* showing transmembrane beta strands. d-e) Distance restraints from a 3D (H)N(H)(H)NH-BASS-SD spectrum of fully protonated U-[$^{13}$C,$^{15}$N]-AlkL protein, recorded at a MAS frequency of 111.11 kHz on a 1GHz spectrometer. d) $^{15}$N-$^{15}$N projection of the 3D spectrum shows the overall high density of cross-peaks. Four strips extracted from the 3D spectrum are shown in e) at the $\delta_2$($^{15}$N) positions indicated by arrows. e) Representative $\delta_1$($^{15}$N)-$\delta_3$($^{1}H^{N}$) strips (at the $\delta_2$($^{15}$N) positions indicated by arrows) contain a number of long-range correlations (highlighted in yellow) in addition to identified sequential peaks. The underlined labels denote auto-correlation signals. Readapted with modification from refs [27, 87].

Figure 8: Figure: Dynamics of KpOmpA β-barrel determined by $^{1}$H-detected solid-state NMR at 60 kHz MAS on a 1 GHz spectrometer. a) assigned $^{1}$H-$^{15}$N correlation spectrum of [$^{1}H^{N}$, $^{2}$H, $^{13}$C, $^{15}$N]-N-KpOmpA reconstituted in lipids. b) topological representation of assigned residues in N-KpOmpA illustrating residue-specific mobility within distinct protein segments and Arg and Lys potential cleavage sites for trypsin. Residues within β-sheet and random coil regions are represented by squares and circles, respectively. Color code: assigned residues are highlighted in green, residues that exhibit intermediate time scale motions are colored in orange, Arg and Lys residues are colored in red, and the unique cleavage site (*i.e.*, R134) accessible to trypsin is highlighted and annotated in red while the surrounding residues within loop 3 are in black. c) representation of β-barrel rocking motion with amplitudes of $\sigma_{//} = 6°$ and $\sigma_{\perp} = 10°$. d-f) respectively, N−H bond order parameters ⟨S⟩, $^{15}$N $R_{1\rho}$ and $R_1$ relaxation rates determined experimentally (red dots) and back-calculated for the rocking motion with $\tau_{GAF}$ = 216 ns (blue bars). Residues for which the agreement is poor (G67, A98, T112, W151) are subject to local motion. Readapted with modification from ref [52].

## References


[1] F. Castellani, B. van Rossum, A. Diehl, M. Schubert, K. Rehbein, H. Oschkinat, Structure of a protein determined by solid-state magic-angle-spinning NMR spectroscopy, Nature 420 (2002) 98-102.

[2] C. Wasmer, A. Lange, H. Van Melckebeke, A.B. Siemer, R. Riek, B.H. Meier, Amyloid fibrils of the HET-s(218-289) prion form a beta solenoid with a triangular hydrophobic core, Science 319 (2008) 1523-6.

[3] Y. Xiao, B. Ma, D. McElheny, S. Parthasarathy, F. Long, M. Hoshi, R. Nussinov, Y. Ishii, Abeta(1-42) fibril structure illuminates self-recognition and replication of amyloid in Alzheimer's disease, Nat Struct Mol Biol 22 (2015) 499-505.

[4] M.T. Colvin, R. Silvers, Q.Z. Ni, T.V. Can, I. Sergeyev, M. Rosay, K.J. Donovan, B. Michael, J. Wall, S. Linse, R.G. Griffin, Atomic Resolution Structure of Monomorphic Aβ42 Amyloid Fibrils, Journal of the American Chemical Society 138 (2016) 9663-74.

[5] M.A. Wälti, F. Ravotti, H. Arai, C.G. Glabe, J.S. Wall, A. Böckmann, P. Güntert, B.H. Meier, R. Riek, Atomic-resolution structure of a disease-relevant Aβ(1-42) amyloid fibril, Proceedings of the National Academy of Sciences of the United States of America 113 (2016) 4976-84.

[6] A. Loquet, N.G. Sgourakis, R. Gupta, K. Giller, D. Riedel, C. Goosmann, C. Griesinger, M. Kolbe, D. Baker, S. Becker, A. Lange, Atomic model of the type III secretion system needle, Nature 486 (2012) 276-9.

[7] I.J. Byeon, G. Hou, Y. Han, C.L. Suiter, J. Ahn, J. Jung, C.H. Byeon, A.M. Gronenborn, T. Polenova, Motions on the millisecond time scale and multiple conformations of HIV-1 capsid protein: implications for structural polymorphism of CA assemblies, J Am Chem Soc 134 (2012) 6455-66.

[8] O. Morag, N.G. Sgourakis, D. Baker, A. Goldbourt, The NMR-Rosetta capsid model of M13 bacteriophage reveals a quadrupled hydrophobic packing epitope, Proc Natl Acad Sci U S A 112 (2015) 971-6.

[9] A. Lange, K. Giller, S. Hornig, M.F. Martin-Eauclaire, O. Pongs, S. Becker, M. Baldus, Toxin-induced conformational changes in a potassium channel revealed by solid-state NMR, Nature 440 (2006) 959-62.

[10] M. Etzkorn, H. Kneuper, P. Dunnwald, V. Vijayan, J. Kramer, C. Griesinger, S. Becker, G. Unden, M. Baldus, Plasticity of the PAS domain and a potential role for signal transduction in the histidine kinase DcuS, Nat Struct Mol Biol 15 (2008) 1031-9.

[11] V.S. Bajaj, M.L. Mak-Jurkauskas, M. Belenky, J. Herzfeld, R.G. Griffin, Functional and shunt states of bacteriorhodopsin resolved by 250 GHz dynamic nuclear polarization-enhanced solid-state NMR, Proc Natl Acad Sci U S A 106 (2009) 9244-9.

[12] M.P. Bhate, A.E. McDermott, Protonation state of E71 in KcsA and its role for channel collapse and inactivation, Proc Natl Acad Sci U S A 109 (2012) 15265-70.

[13] M. Tang, A.E. Nesbitt, L.J. Sperling, D.A. Berthold, C.D. Schwieters, R.B. Gennis, C.M. Rienstra, Structure of the disulfide bond generating membrane protein DsbB in the lipid bilayer, J Mol Biol 425 (2013) 1670-82.

[14] B.J. Wylie, M.P. Bhate, A.E. McDermott, Transmembrane allosteric coupling of the gates in a potassium channel, Proc Natl Acad Sci U S A 111 (2014) 185-90.

[15] R. Huang, K. Yamamoto, M. Zhang, N. Popovych, I. Hung, S.C. Im, Z. Gan, L. Waskell, A. Ramamoorthy, Probing the transmembrane structure and dynamics of microsomal NADPH-cytochrome P450 oxidoreductase by solid-state NMR, Biophys J 106 (2014) 2126-33.

[16] J. Becker-Baldus, C. Bamann, K. Saxena, H. Gustmann, L.J. Brown, R.C. Brown, C. Reiter, E. Bamberg, J. Wachtveitl, H. Schwalbe, C. Glaubitz, Enlightening the photoactive site of channelrhodopsin-2 by DNP-enhanced solid-state NMR spectroscopy, Proc Natl Acad Sci U S A 112 (2015) 9896-901.

[17] J. Hu, T. Asbury, S. Achuthan, C. Li, R. Bertram, J.R. Quine, R. Fu, T.A. Cross, Backbone structure of the amantadine-blocked trans-membrane domain M2 proton channel from Influenza A virus, Biophys J 92 (2007) 4335-43.

[18] S.D. Cady, K. Schmidt-Rohr, J. Wang, C.S. Soto, W.F. Degrado, M. Hong, Structure of the amantadine binding site of influenza M2 proton channels in lipid bilayers, Nature 463 (2010) 689-92.
[19] M. Renault, R. Tommassen-van Boxtel, M.P. Bos, J.A. Post, J. Tommassen, M. Baldus, Cellular solid-state nuclear magnetic resonance spectroscopy, Proc Natl Acad Sci U S A 109 (2012) 4863-8.
[20] Y. Miao, H. Qin, R. Fu, M. Sharma, T.V. Can, I. Hung, S. Luca, P.L. Gor'kov, W.W. Brey, T.A. Cross, M2 proton channel structural validation from full-length protein samples in synthetic bilayers and E. coli membranes, Angew Chem Int Ed Engl 51 (2012) 8383-6.
[21] M.E. Ward, S. Wang, R. Munro, E. Ritz, I. Hung, P.L. Gor'kov, Y. Jiang, H. Liang, L.S. Brown, V. Ladizhansky, In situ structural studies of Anabaena sensory rhodopsin in the E. coli membrane, Biophys J 108 (2015) 1683-96.
[22] S. Wang, V. Ladizhansky, Recent advances in magic angle spinning solid state NMR of membrane proteins, Prog Nucl Magn Reson Spectrosc 82 (2014) 1-26.
[23] N.J. Traaseth, L. Shi, R. Verardi, D.G. Mullen, G. Barany, G. Veglia, Structure and topology of monomeric phospholamban in lipid membranes determined by a hybrid solution and solid-state NMR approach, Proc Natl Acad Sci U S A 106 (2009) 10165-70.
[24] B.B. Das, H.J. Nothnagel, G.J. Lu, W.S. Son, Y. Tian, F.M. Marassi, S.J. Opella, Structure determination of a membrane protein in proteoliposomes, J Am Chem Soc 134 (2012) 2047-56.
[25] S.H. Park, B.B. Das, F. Casagrande, Y. Tian, H.J. Nothnagel, M. Chu, H. Kiefer, K. Maier, A.A. De Angelis, F.M. Marassi, S.J. Opella, Structure of the chemokine receptor CXCR1 in phospholipid bilayers, Nature 491 (2012) 779-83.
[26] S. Wang, R.A. Munro, L. Shi, I. Kawamura, T. Okitsu, A. Wada, S.Y. Kim, K.H. Jung, L.S. Brown, V. Ladizhansky, Solid-state NMR spectroscopy structure determination of a lipid-embedded heptahelical membrane protein, Nat Methods 10 (2013) 1007-12.
[27] L.B. Andreas, M. Reese, M.T. Eddy, V. Gelev, Q.Z. Ni, E.A. Miller, L. Emsley, G. Pintacuda, J.J. Chou, R.G. Griffin, Structure and Mechanism of the Influenza A M218-60 Dimer of Dimers, J Am Chem Soc 137 (2015) 14877-86.
[28] R. Ketchem, B. Roux, T. Cross, High-resolution polypeptide structure in a lamellar phase lipid environment from solid state NMR derived orientational constraints, Structure 5 (1997) 1655-69.
[29] S.H. Park, A.A. Mrse, A.A. Nevzorov, M.F. Mesleh, M. Oblatt-Montal, M. Montal, S.J. Opella, Three-dimensional structure of the channel-forming trans-membrane domain of virus protein "u" (Vpu) from HIV-1, J Mol Biol 333 (2003) 409-24.
[30] C.M. Rienstra, M. Hohwy, M. Hong, R.G. Griffin, 2D and 3D 15N-13C-13C NMR Chemical Shift Correlation Spectroscopy of Solids: Assignment of MAS Spectra of Peptides, J Am Chem Soc 122 (2000) 10979-10990.
[31] A. Bockmann, A. Lange, A. Galinier, S. Luca, N. Giraud, M. Juy, H. Heise, R. Montserret, F. Penin, M. Baldus, Solid state NMR sequential resonance assignments and conformational analysis of the 2x10.4 kDa dimeric form of the Bacillus subtilis protein Crh, J Biomol NMR 27 (2003) 323-39.
[32] M. Sattler, J. Schleucher, C. Griesinger, Heteronuclear multidimensional NMR experiments for the structure determination of proteins in solution employing pulsed field gradients, Prog Nucl Magn Reson Spectrosc 34 (1999) 93-158.
[33] P. Guerry, T. Herrmann, Advances in automated NMR protein structure determination, Q Rev Biophys 44 (2011) 257-309.
[34] Y. Ishii, R. Tycko, Sensitivity enhancement in solid state (15)N NMR by indirect detection with high-speed magic angle spinning, J Magn Reson 142 (2000) 199-204.
[35] A. Samoson, T. Tuherm, Z. Gan, High-field high-speed MAS resolution enhancement in 1H NMR spectroscopy of solids, Solid State Nucl Magn Reson 20 (2001) 130-6.

[36] Y. Ishii, J.P. Yesinowski, R. Tycko, Sensitivity enhancement in solid-state (13)C NMR of synthetic polymers and biopolymers by (1)H NMR detection with high-speed magic angle spinning, J Am Chem Soc 123 (2001) 2921-2.
[37] L. Zheng, K.W. Fishbein, R.G. Griffin, J. Herzfeld, Two-dimensional solid-state proton NMR and proton exchange, J Am Chem Soc 115 (1993) 6254-6261.
[38] B. Reif, C.P. Jaroniec, C.M. Rienstra, M. Hohwy, R.G. Griffin, 1H-1H MAS correlation spectroscopy and distance measurements in a deuterated peptide. Journal of Magnetic Resonance, J Magn Reson 151 (2001 ) 320-7.
[39] E.K. Paulson, C.R. Morcombe, V. Gaponenko, B. Dancheck, R.A. Byrd, K.W. Zilm, Sensitive high resolution inverse detection NMR spectroscopy of proteins in the solid state, J Am Chem Soc 125 (2003) 15831-6.
[40] V. Chevelkov, K. Rehbein, A. Diehl, B. Reif, Ultrahigh resolution in proton solid-state NMR spectroscopy at high levels of deuteration, Angew Chem Int Ed Engl 45 (2006) 3878-81.
[41] R. Linser, M. Dasari, M. Hiller, V. Higman, U. Fink, J.M. Lopez del Amo, S. Markovic, L. Handel, B. Kessler, P. Schmieder, D. Oesterhelt, H. Oschkinat, B. Reif, Proton-detected solid-state NMR spectroscopy of fibrillar and membrane proteins, Angew Chem Int Ed Engl 50 (2011) 4508-12.
[42] U. Akbey, S. Lange, W. Trent Franks, R. Linser, K. Rehbein, A. Diehl, B.J. van Rossum, B. Reif, H. Oschkinat, Optimum levels of exchangeable protons in perdeuterated proteins for proton detection in MAS solid-state NMR spectroscopy, J Biomol NMR 46 (2010) 67-73.
[43] M.E. Ward, L. Shi, E. Lake, S. Krishnamurthy, H. Hutchins, L.S. Brown, V. Ladizhansky, Proton-detected solid-state NMR reveals intramembrane polar networks in a seven-helical transmembrane protein proteorhodopsin, J Am Chem Soc 133 (2011) 17434-43.
[44] D.H. Zhou, A.J. Nieuwkoop, D.A. Berthold, G. Comellas, L.J. Sperling, M. Tang, G.J. Shah, E.J. Brea, L.R. Lemkau, C.M. Rienstra, Solid-state NMR analysis of membrane proteins and protein aggregates by proton detected spectroscopy, J Biomol NMR 54 (2012) 291-305.
[45] J.R. Lewandowski, J.-N. Dumez, U. Akbey, A. Lange, L. Emsley, H. Oschkinat, Enhanced resolution and coherence lifetimes in the solid-state NMR spectroscopy of perdeuterated proteins under ultrafast magic-angle spinning J Phys Chem Lett 2 (2011) 2205-2211.
[46] M.J. Knight, A.L. Webber, A.J. Pell, P. Guerry, E. Barbet-Massin, I. Bertini, I.C. Felli, L. Gonnelli, R. Pierattelli, L. Emsley, A. Lesage, T. Herrmann, G. Pintacuda, Fast resonance assignment and fold determination of human superoxide dismutase by high-resolution proton-detected solid-state MAS NMR spectroscopy, Angew Chem Int Ed Engl 50 (2011) 11697-701.
[47] L.B. Andreas, T. Le Marchand, K. Jaudzems, G. Pintacuda, High-resolution proton-detected NMR of proteins at very fast MAS, J Magn Reson 253 (2015) 36-49.
[48] A.J. Nieuwkoop, W.T. Franks, K. Rehbein, A. Diehl, U. Akbey, F. Engelke, L. Emsley, G. Pintacuda, H. Oschkinat, Sensitivity and resolution of proton detected spectra of a deuterated protein at 40 and 60 kHz magic-angle-spinning, J Biomol NMR 61 (2015) 161-71.
[49] E. Barbet-Massin, A.J. Pell, J.S. Retel, L.B. Andreas, K. Jaudzems, W.T. Franks, A.J. Nieuwkoop, M. Hiller, V. Higman, P. Guerry, A. Bertarello, M.J. Knight, M. Felletti, T. Le Marchand, S. Kotelovica, I. Akopjana, K. Tars, M. Stoppini, V. Bellotti, M. Bolognesi, S. Ricagno, J.J. Chou, R.G. Griffin, H. Oschkinat, A. Lesage, L. Emsley, T. Herrmann, G. Pintacuda, Rapid proton-detected NMR assignment for proteins with fast magic angle spinning, J Am Chem Soc 136 (2014) 12489-97.
[50] M.J. Knight, A.J. Pell, I. Bertini, I.C. Felli, L. Gonnelli, R. Pierattelli, T. Herrmann, L. Emsley, G. Pintacuda, Structure and backbone dynamics of a microcrystalline metalloprotein by solid-state NMR, Proc Natl Acad Sci U S A 109 (2012) 11095-100.
[51] J.S. Retel, A.J. Nieuwkoop, M. Hiler, V.A. Higman, E. Barbet-Massin, J. Stanek, L.B. Andreas, W.T. Franks, B.-J. van Rossum, K.R. Vinothkumar, L. Handel, B. Bardiaux, G. Pintacuda, L. Emsley, W. Kühlbrandt, H. Oschkinat, Structure of Outer Membrane Protein G (OmpG) in native lipids, Nat Commun in press (2017).

[52] O. Saurel, I. Iordanov, G. Nars, P. Demange, T. Le Marchand, L.B. Andreas, G. Pintacuda, A. Milon, Local and Global Dynamics in Klebsiella pneumoniae Outer Membrane Protein a in Lipid Bilayers Probed at Atomic Resolution, J Am Chem Soc 139 (2017) 1590-1597.
[53] M.T. Eddy, Y. Su, R. Silvers, L. Andreas, L. Clark, G. Wagner, G. Pintacuda, L. Emsley, R.G. Griffin, Lipid bilayer-bound conformation of an integral membrane beta barrel protein by multidimensional MAS NMR, J Biomol NMR 61 (2015) 299-310.
[54] J.M. Lamley, D. Iuga, C. Oster, H.J. Sass, M. Rogowski, A. Oss, J. Past, A. Reinhold, S. Grzesiek, A. Samoson, J.R. Lewandowski, Solid-state NMR of a protein in a precipitated complex with a full-length antibody, J Am Chem Soc 136 (2014) 16800-6.
[55] V. Agarwal, S. Penzel, K. Szekely, R. Cadalbert, E. Testori, A. Oss, J. Past, A. Samoson, M. Ernst, A. Bockmann, B.H. Meier, De novo 3D structure determination from sub-milligram protein samples by solid-state 100 kHz MAS NMR spectroscopy, Angew Chem Int Ed Engl 53 (2014) 12253-6.
[56] L.B. Andreas, J. Stanek, T. Le Marchand, A. Bertarello, D. Cala-De Paepe, D. Lalli, M. Krejcikova, C. Doyen, C. Oster, B. Knott, S. Wegner, F. Engelke, I.C. Felli, R. Pierattelli, N.E. Dixon, L. Emsley, T. Herrmann, G. Pintacuda, Protein residue linking in a single spectrum for magic-angle spinning NMR assignment, J Biomol NMR 62 (2015) 253-61.
[57] K.H. Mroue, Y. Nishiyama, M. Kumar Pandey, B. Gong, E. McNerny, D.H. Kohn, M.D. Morris, A. Ramamoorthy, Proton-Detected Solid-State NMR Spectroscopy of Bone with Ultrafast Magic Angle Spinning, Sci Rep 5 (2015) 11991.
[58] L.B. Andreas, K. Jaudzems, J. Stanek, D. Lalli, A. Bertarello, T. Le Marchand, D. Cala-De Paepe, S. Kotelovica, I. Akopjana, B. Knott, S. Wegner, F. Engelke, A. Lesage, L. Emsley, K. Tars, T. Herrmann, G. Pintacuda, Structure of fully protonated proteins by proton-detected magic-angle spinning NMR, Proc Natl Acad Sci U S A 113 (2016) 9187-92.
[59] Y. Nishiyama, Fast magic-angle sample spinning solid-state NMR at 60-100kHz for natural abundance samples, Solid State Nucl Magn Reson 78 (2016) 24-36.
[60] D. Cala-De Paepe, J. Stanek, K. Jaudzems, K. Tars, L.B. Andreas, G. Pintacuda, Is protein deuteration beneficial for proton detected solid-state NMR at and above 100 kHz magic-angle spinning?, Solid State Nucl Magn Reson (2017).
[61] J. Medeiros-Silva, D. Mance, M. Daniels, S. Jekhmane, K. Houben, M. Baldus, M. Weingarth, 1 H-Detected Solid-State NMR Studies of Water-Inaccessible Proteins In Vitro and In Situ, Angew Chem Int Ed Engl 55 (2016) 13606-13610.
[62] D. Lalli, M.N. Idso, L.B. Andreas, S. Hussain, N. Baxter, S. Han, B.F. Chmelka, G. Pintacuda, Proton-Based Structural Analysis of a Heptahelical Transmembrane Protein in Lipid Bilayers, J Am Chem Soc 139 (2017) 13006-13012.
[63] S. Asami, P. Schmieder, B. Reif, High resolution 1H-detected solid-state NMR spectroscopy of protein aliphatic resonances: access to tertiary structure information, J Am Chem Soc 132 (2010) 15133-5.
[64] D. Nand, A. Cukkemane, S. Becker, M. Baldus, Fractional deuteration applied to biomolecular solid-state NMR spectroscopy, J Biomol NMR 52 (2012) 91-101.
[65] D. Mance, T. Sinnige, M. Kaplan, S. Narasimhan, M. Daniels, K. Houben, M. Baldus, M. Weingarth, An Efficient Labelling Approach to Harness Backbone and Side-Chain Protons in (1) H-Detected Solid-State NMR Spectroscopy, Angew Chem Int Ed Engl 54 (2015) 15799-803.
[66] Y. Yao, S.K. Dutta, S.H. Park, R. Rai, L.M. Fujimoto, A.A. Bobkov, S.J. Opella, F.M. Marassi, High resolution solid-state NMR spectroscopy of the Yersinia pestis outer membrane protein Ail in lipid membranes, J Biomol NMR 67 (2017) 179-190.
[67] S. Asami, K. Szekely, P. Schanda, B.H. Meier, B. Reif, Optimal degree of protonation for (1)H detection of aliphatic sites in randomly deuterated proteins as a function of the MAS frequency, J Biomol NMR 54 (2012) 155-68.
[68] M. Huber, S. Hiller, P. Schanda, M. Ernst, A. Bockmann, R. Verel, B.H. Meier, A proton-detected 4D solid-state NMR experiment for protein structure determination, Chemphyschem 12 (2011) 915-8.

[69] T. Sinnige, M. Daniels, M. Baldus, M. Weingarth, Proton clouds to measure long-range contacts between nonexchangeable side chain protons in solid-state NMR, J Am Chem Soc 136 (2014) 4452-5.
[70] D.H. Zhou, G. Shah, M. Cormos, C. Mullen, D. Sandoz, C.M. Rienstra, Proton-detected solid-state NMR spectroscopy of fully protonated proteins at 40 kHz magic-angle spinning, J Am Chem Soc 129 (2007) 11791-801.
[71] A. Marchetti, S. Jehle, M. Felletti, M.J. Knight, Y. Wang, Z.Q. Xu, A.Y. Park, G. Otting, A. Lesage, L. Emsley, N.E. Dixon, G. Pintacuda, Backbone assignment of fully protonated solid proteins by 1H detection and ultrafast magic-angle-spinning NMR spectroscopy, Angew Chem Int Ed Engl 51 (2012) 10756-9.
[72] S. Xiang, J. Biernat, E. Mandelkow, S. Becker, R. Linser, Backbone assignment for minimal protein amounts of low structural homogeneity in the absence of deuteration, Chem Commun (Camb) 52 (2016) 4002-5.
[73] J. Stanek, L.B. Andreas, K. Jaudzems, D. Cala, D. Lalli, A. Bertarello, T. Schubeis, I. Akopjana, S. Kotelovica, K. Tars, A. Pica, S. Leone, D. Picone, Z.Q. Xu, N.E. Dixon, D. Martinez, M. Berbon, N. El Mammeri, A. Noubhani, S. Saupe, B. Habenstein, A. Loquet, G. Pintacuda, NMR Spectroscopic Assignment of Backbone and Side-Chain Protons in Fully Protonated Proteins: Microcrystals, Sedimented Assemblies, and Amyloid Fibrils, Angew Chem Int Ed Engl 55 (2016) 15504-15509.
[74] N. Das, D.T. Murray, T.A. Cross, Lipid bilayer preparations of membrane proteins for oriented and magic-angle spinning solid-state NMR samples, Nat Protoc 8 (2013) 2256-70.
[75] A. Bockmann, C. Gardiennet, R. Verel, A. Hunkeler, A. Loquet, G. Pintacuda, L. Emsley, B.H. Meier, A. Lesage, Characterization of different water pools in solid-state NMR protein samples, J Biomol NMR 45 (2009) 319-27.
[76] I. Bertini, F. Engelke, L. Gonnelli, B. Knott, C. Luchinat, D. Osen, E. Ravera, On the use of ultracentrifugal devices for sedimented solute NMR, J Biomol NMR 54 (2012) 123-7.
[77] D.T. Murray, J. Griffin, T.A. Cross, Detergent optimized membrane protein reconstitution in liposomes for solid state NMR, Biochemistry 53 (2014) 2454-63.
[78] T.S. Schwarzer, M. Hermann, S. Krishnan, F.C. Simmel, K. Castiglione, Preparative refolding of small monomeric outer membrane proteins, Protein Expr Purif 132 (2017) 171-181.
[79] P. Fricke, V. Chevelkov, M. Zinke, K. Giller, S. Becker, A. Lange, Backbone assignment of perdeuterated proteins by solid-state NMR using proton detection and ultrafast magic-angle spinning, Nat Protoc 12 (2017) 764-782.
[80] D.H. Zhou, J.J. Shea, A.J. Nieuwkoop, W.T. Franks, B.J. Wylie, C. Mullen, D. Sandoz, C.M. Rienstra, Solid-state protein-structure determination with proton-detected triple-resonance 3D magic-angle-spinning NMR spectroscopy, Angew Chem Int Ed Engl 46 (2007) 8380-3.
[81] I. Bertini, L. Emsley, I.C. Felli, S. Laage, A. Lesage, J.R. Lewandowski, A. Marchetti, R. Pierattelli, G. Pintacuda, High-resolution and sensitivity through-bond correlations in ultra-fast magic angle spinning (MAS) solid-state NMR, Chemical Science 2 (2011) 345-348.
[82] E. Barbet-Massin, A.J. Pell, K. Jaudzems, W.T. Franks, J.S. Retel, S. Kotelovica, I. Akopjana, K. Tars, L. Emsley, H. Oschkinat, A. Lesage, G. Pintacuda, Out-and-back 13C-13C scalar transfers in protein resonance assignment by proton-detected solid-state NMR under ultra-fast MAS, J Biomol NMR 56 (2013) 379-86.
[83] J. Volk, T. Herrmann, K. Wuthrich, Automated sequence-specific protein NMR assignment using the memetic algorithm MATCH, J Biomol NMR 41 (2008) 127-38.
[84] E. Schmidt, P. Guntert, A new algorithm for reliable and general NMR resonance assignment, J Am Chem Soc 134 (2012) 12817-29.
[85] S. Xiang, K. Grohe, P. Rovo, S.K. Vasa, K. Giller, S. Becker, R. Linser, Sequential backbone assignment based on dipolar amide-to-amide correlation experiments, J Biomol NMR 62 (2015) 303-11.

[86] P.L. Gor'kov, E.Y. Chekmenev, C. Li, M. Cotten, J.J. Buffy, N.J. Traaseth, G. Veglia, W.W. Brey, Using low-E resonators to reduce RF heating in biological samples for static solid-state NMR up to 900 MHz, J Magn Reson 185 (2007) 77-93.
[87] M.G. Jain, D. Lalli, J. Stanek, C. Gowda, S. Prakash, T.S. Schwarzer, T. Schubeis, K. Castiglione, L.B. Andreas, P.K. Madhu, G. Pintacuda, V. Agarwal, Selective 1H-1H Distance Restraints in Fully Protonated Proteins by Very Fast Magic-Angle Spinning Solid-State NMR, J Phys Chem Lett 8 (2017) 2399-2405.
[88] M. Sharma, M. Yi, H. Dong, H. Qin, E. Peterson, D.D. Busath, H.X. Zhou, T.A. Cross, Insight into the mechanism of the influenza A proton channel from a structure in a lipid bilayer, Science 330 (2010) 509-12.
[89] A.L. Stouffer, R. Acharya, D. Salom, A.S. Levine, L. Di Costanzo, C.S. Soto, V. Tereshko, V. Nanda, S. Stayrook, W.F. DeGrado, Structural basis for the function and inhibition of an influenza virus proton channel, Nature 451 (2008) 596-9.
[90] J.R. Schnell, J.J. Chou, Structure and mechanism of the M2 proton channel of influenza A virus, Nature 451 (2008) 591-5.
[91] M. Dolder, K. Zeth, P. Tittmann, H. Gross, W. Welte, T. Wallimann, Crystallization of the human, mitochondrial voltage-dependent anion-selective channel in the presence of phospholipids, J Struct Biol 127 (1999) 64-71.
[92] G.V. Subbarao, B. van den Berg, Crystal structure of the monomeric porin OmpG, J Mol Biol 360 (2006) 750-9.
[93] M. Hiller, L. Krabben, K.R. Vinothkumar, F. Castellani, B.J. van Rossum, W. Kuhlbrandt, H. Oschkinat, Solid-state magic-angle spinning NMR of outer-membrane protein G from Escherichia coli, Chembiochem 6 (2005) 1679-84.
[94] C. Grant, D. Deszcz, Y.C. Wei, R.J. Martinez-Torres, P. Morris, T. Folliard, R. Sreenivasan, J. Ward, P. Dalby, J.M. Woodley, F. Baganz, Identification and use of an alkane transporter plug-in for applications in biocatalysis and whole-cell biosensing of alkanes, Sci Rep 4 (2014) 5844.
[95] J.J. Wittmann, V. Agarwal, J. Hellwagner, A. Lends, R. Cadalbert, B.H. Meier, M. Ernst, Accelerating proton spin diffusion in perdeuterated proteins at 100 kHz MAS, J Biomol NMR 66 (2016) 233-242.
[96] P. Schanda, B.H. Meier, M. Ernst, Quantitative analysis of protein backbone dynamics in microcrystalline ubiquitin by solid-state NMR spectroscopy, J Am Chem Soc 132 (2010) 15957-67.
[97] S. Asami, J.R. Porter, O.F. Lange, B. Reif, Access to Calpha backbone dynamics of biological solids by 13C T1 relaxation and molecular dynamics simulation, J Am Chem Soc 137 (2015) 1094-100.
[98] J.M. Lamley, M.J. Lougher, H.J. Sass, M. Rogowski, S. Grzesiek, J.R. Lewandowski, Unraveling the complexity of protein backbone dynamics with combined (13)C and (15)N solid-state NMR relaxation measurements, Phys Chem Chem Phys 17 (2015) 21997-2008.
[99] D.F. Gauto, A. Hessel, P. Rovo, V. Kurauskas, R. Linser, P. Schanda, Protein conformational dynamics studied by 15N and 1H R1rho relaxation dispersion: Application to wild-type and G53A ubiquitin crystals, Solid State Nucl Magn Reson (2017).
[100] J.R. Lewandowski, H.J. Sass, S. Grzesiek, M. Blackledge, L. Emsley, Site-specific measurement of slow motions in proteins, J Am Chem Soc 133 (2011) 16762-5.
[101] P. Ma, J.D. Haller, J. Zajakala, P. Macek, A.C. Sivertsen, D. Willbold, J. Boisbouvier, P. Schanda, Probing transient conformational states of proteins by solid-state R(1rho) relaxation-dispersion NMR spectroscopy, Angew Chem Int Ed Engl 53 (2014) 4312-7.
[102] H.R. Dannatt, M. Felletti, S. Jehle, Y. Wang, L. Emsley, N.E. Dixon, A. Lesage, G. Pintacuda, Weak and Transient Protein Interactions Determined by Solid-State NMR, Angew Chem Int Ed Engl 55 (2016) 6638-41.
[103] A.A. Smith, E. Testori, R. Cadalbert, B.H. Meier, M. Ernst, Characterization of fibril dynamics on three timescales by solid-state NMR, J Biomol NMR 65 (2016) 171-91.

[104] D.B. Good, S. Wang, M.E. Ward, J. Struppe, L.S. Brown, J.R. Lewandowski, V. Ladizhansky, Conformational dynamics of a seven transmembrane helical protein Anabaena Sensory Rhodopsin probed by solid-state NMR, J Am Chem Soc 136 (2014) 2833-42.
[105] B. Bersch, J.M. Dorr, A. Hessel, J.A. Killian, P. Schanda, Proton-Detected Solid-State NMR Spectroscopy of a Zinc Diffusion Facilitator Protein in Native Nanodiscs, Angew Chem Int Ed Engl 56 (2017) 2508-2512.
[106] N.A. Lakomek, L. Frey, S. Bibow, A. Bockmann, R. Riek, B.H. Meier, Proton-Detected NMR Spectroscopy of Nanodisc-Embedded Membrane Proteins: MAS Solid-State vs Solution-State Methods, J Phys Chem B 121 (2017) 7671-7680.
[107] H.R. Dannatt, G.F. Taylor, K. Varga, V.A. Higman, M.P. Pfeil, L. Asilmovska, P.J. Judge, A. Watts, 13C- and 1H-detection under fast MAS for the study of poorly available proteins: application to sub-milligram quantities of a 7 trans-membrane protein, J Biomol NMR 62 (2015) 17-23.

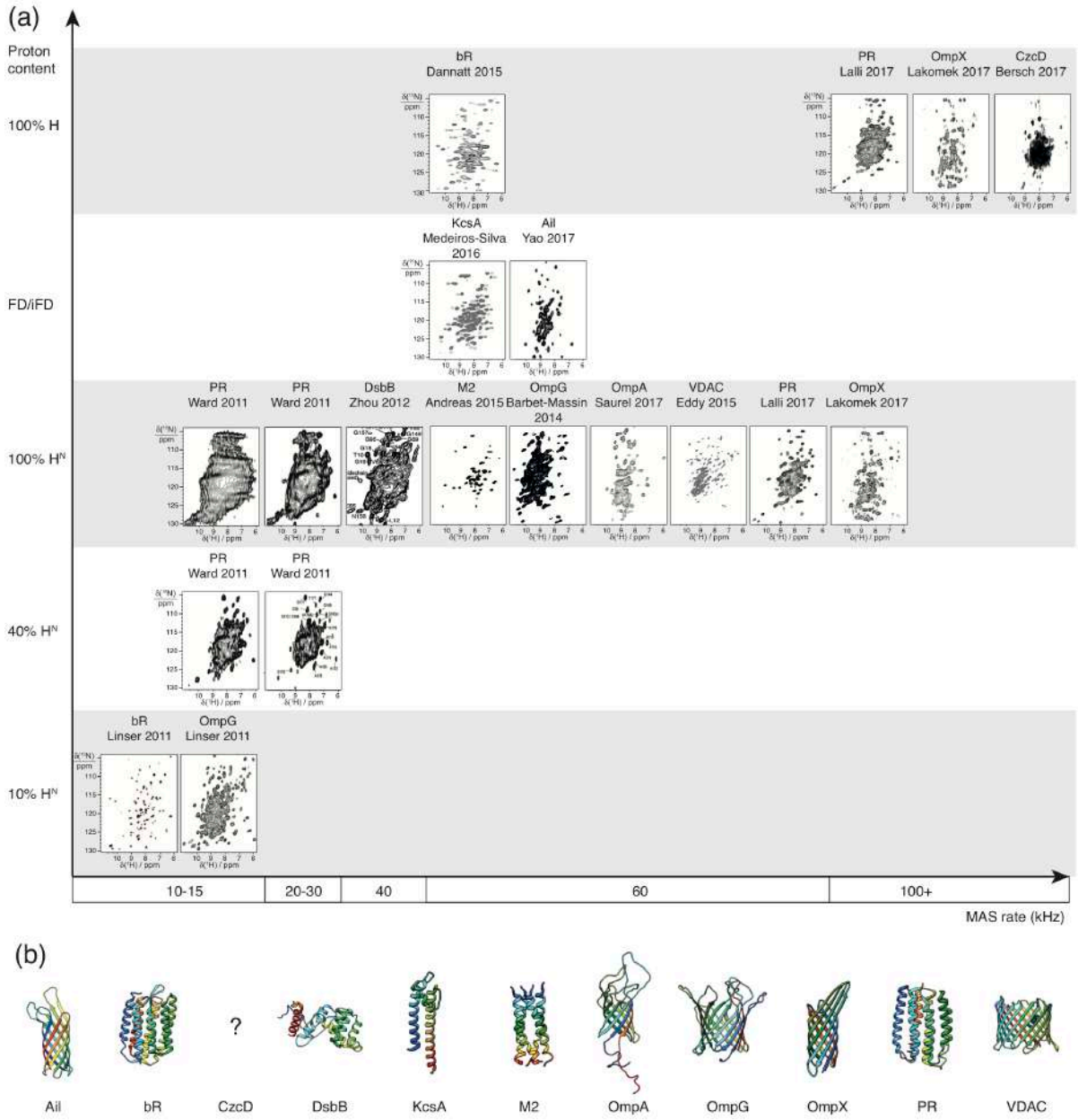


**Figure 1**

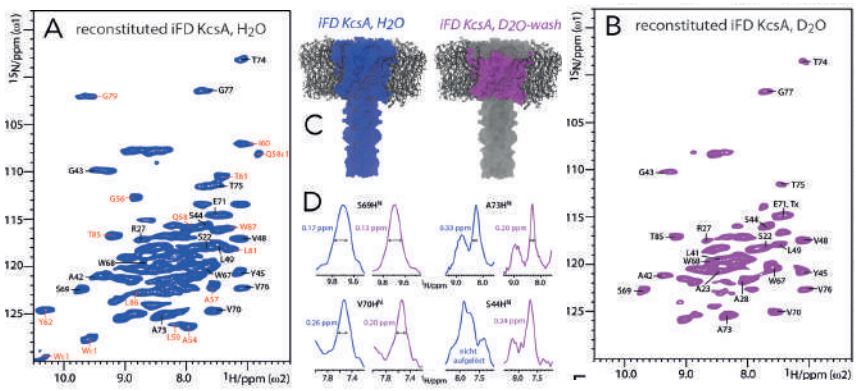


**Figure 2**

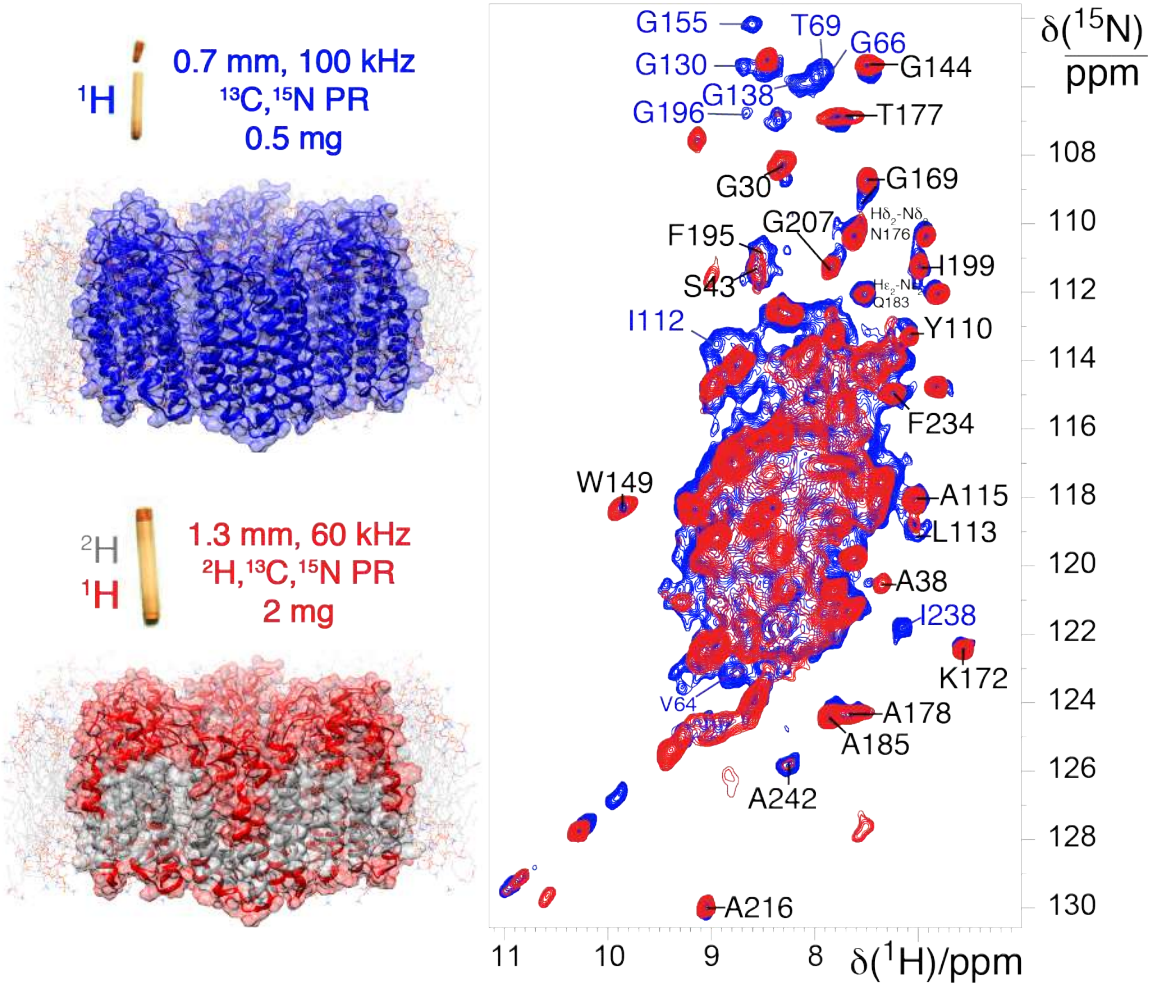


**Figure 3**

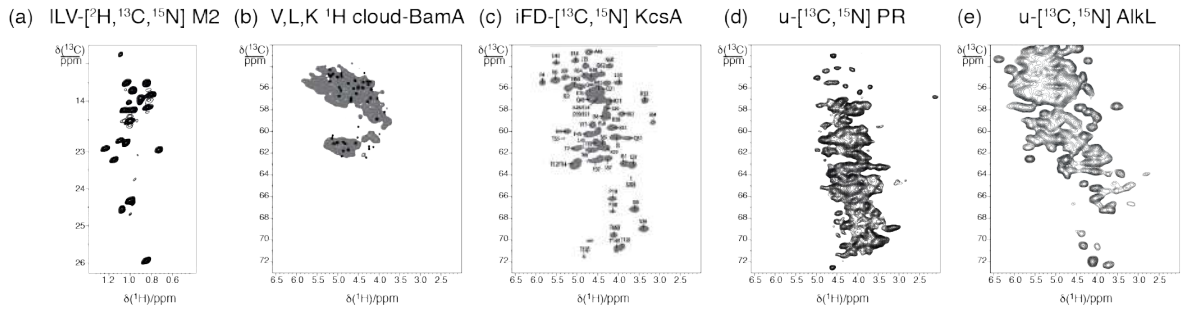


**Figure 4**

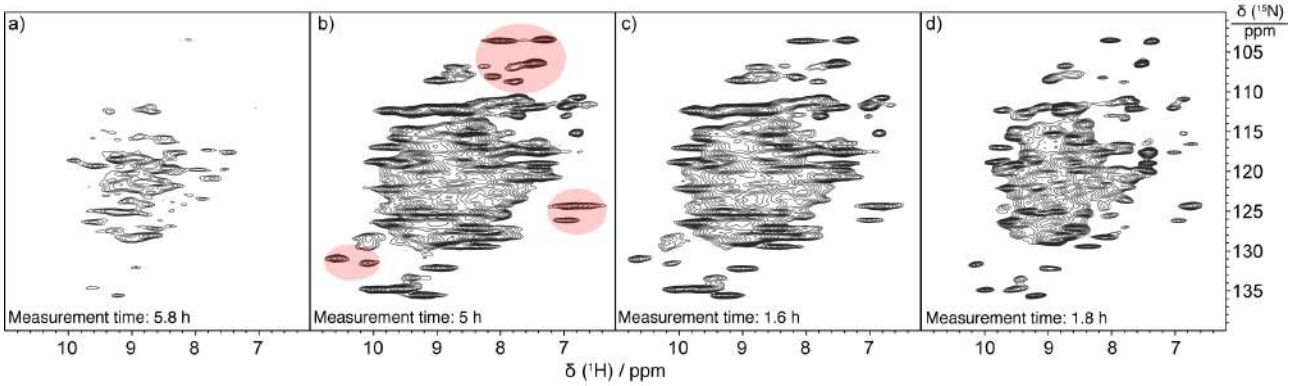


**Figure 5**

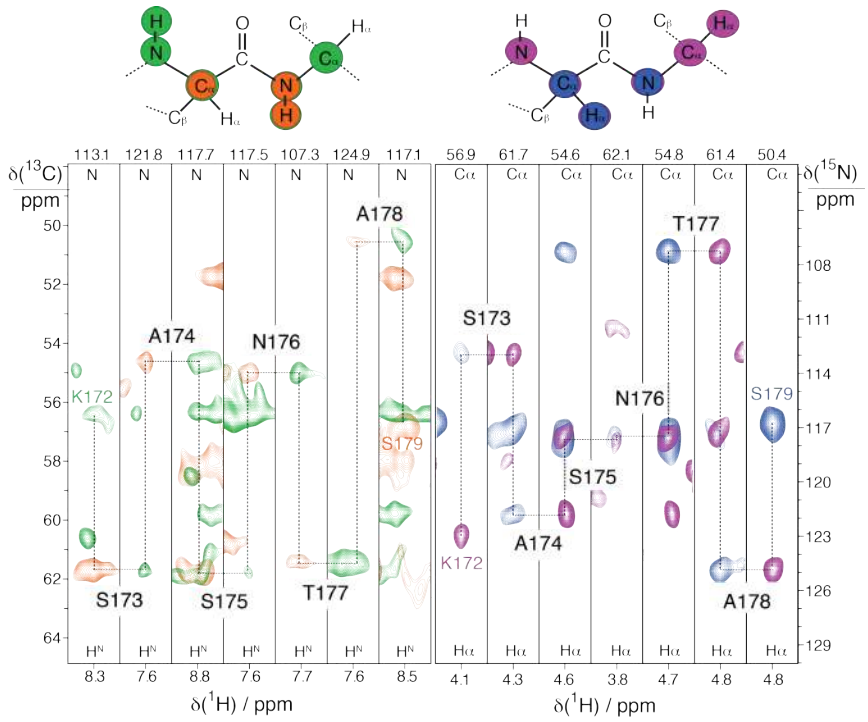


**Figure 6**

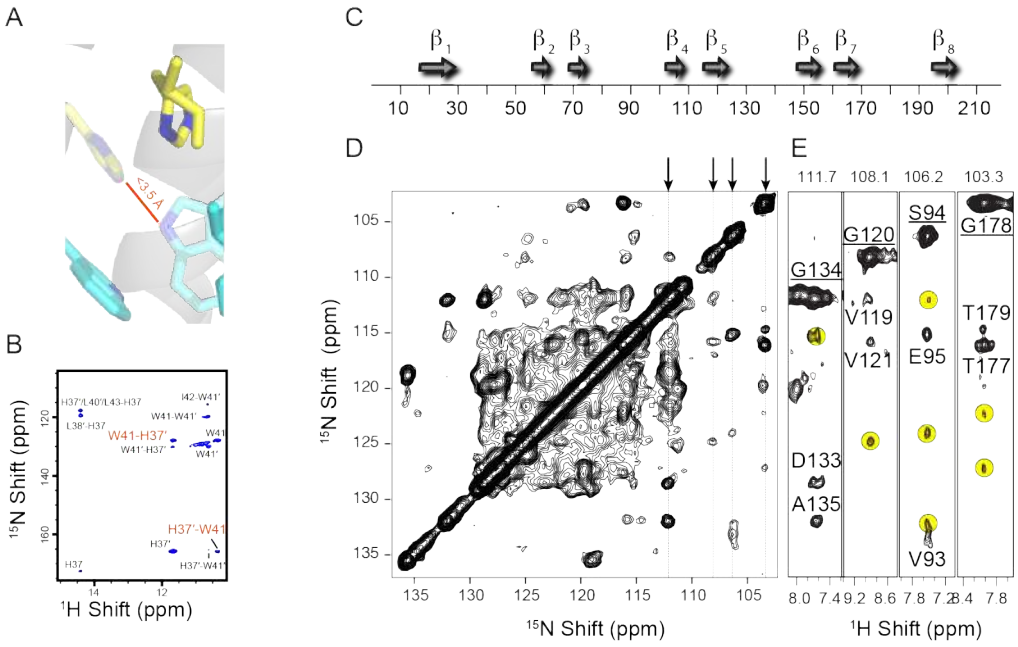


**Figure 7**

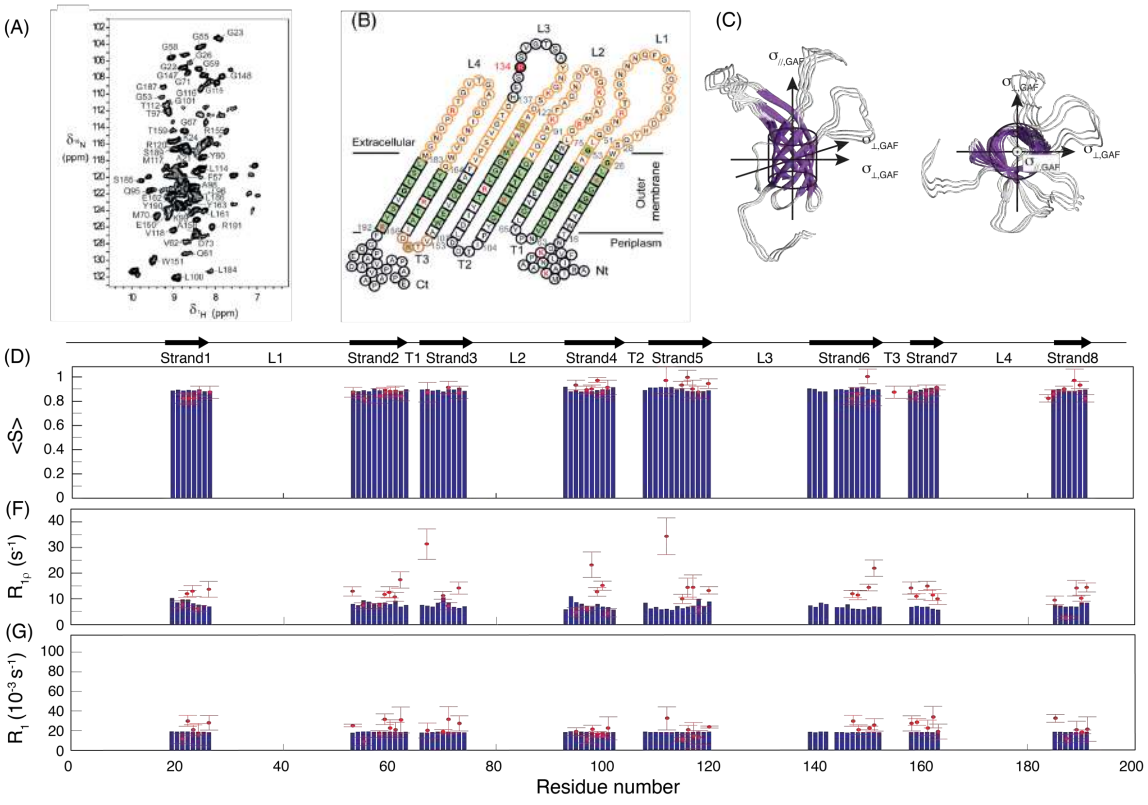


**Figure 8**